UNITED NATIONS UNIVERSITY
GEOTHERMAL TRAINING PROGRAMME
Orkustofnun, Grensásvegur 9,
IS-108 Reykjavík, Iceland

Reports 2009
Number 26

THREE-DIMENSIONAL MODEL OF THE NIUTUOZHEN GEOTHERMAL SYSTEM, HEBEI PROVINCE, CHINA

Wang Shufang
Beijing Institute of Geological Engineering
No.90, Beiwa Road
Beijing 100048
P.R. CHINA
Shufangwang111@163.com

ABSTRACT

The Niutuozhen geothermal system, located in North China, is composed of the Jixian system dolomite reservoir and a Neogene sandstone reservoir. A three-dimensional model with 5437 elements and seven layers based on the geological and geothermal data was built using the AQUA3D package designed for solving flow and transport problems. An area of 1050 km^2 confined by four faults is included in the model. Production history of forty five wells and pressure monitoring data from six wells were used for calibration. Permeability was estimated to range from 2.5 to 25×10^{-16} m^2 in layer 6 after a satisfying agreement was obtained between the measured and computed water level data. The maximum predicted drawdown after 20 years of production without any reinjection ranged from 30 to 120 m in the north and south, respectively. The rate of drawdown was predicted to be kept at a lower level if 50% of the produced water was reinjected into the system. Cones of depression were predicted to gradually enlarge due to an increased production rate without reinjection, but were effectively limited and even diminished with a reinjection ratio of 50%. A maximum temperature decrease of 2.75°C was predicted to occur in production well A34, located near the reinjection well R3, for a production rate of 162 l/s with 50% reinjection. The maximum temperature decrease of 24.81°C was predicted to occur in the southern reinjection well R2. The cooling plumes surrounding the reinjection wells were predicted to gradually enlarge with an increasing reinjection fraction. Prediction of temperature response indicated that the reinjection rate, the temperature of the reinjected water and the distance between the reinjection and production wells are the three factors affecting the reservoir temperature change.

1. INTRODUCTION

The Niutuozhen geothermal system is a low-enthalpy geothermal system, located in the North China fault basin of uplifted bedrock in the centre of Hebei province, including part of Xiongxian, Rongcheng, Yongqing, Anxin, Gu'an and Baxian (Figure 1). It was discovered in the 1970s during petroleum exploration. Previous research, dating back to the 1980s, dealing with geological background, thermal conditions, geothermal reservoirs and geothermal development, suggests that the Niutuozhen geothermal field is one of the largest geothermal fields in North China and is capable of sustaining a high level of geothermal energy production (Chen et al., 1982; Chen et al., 1985;

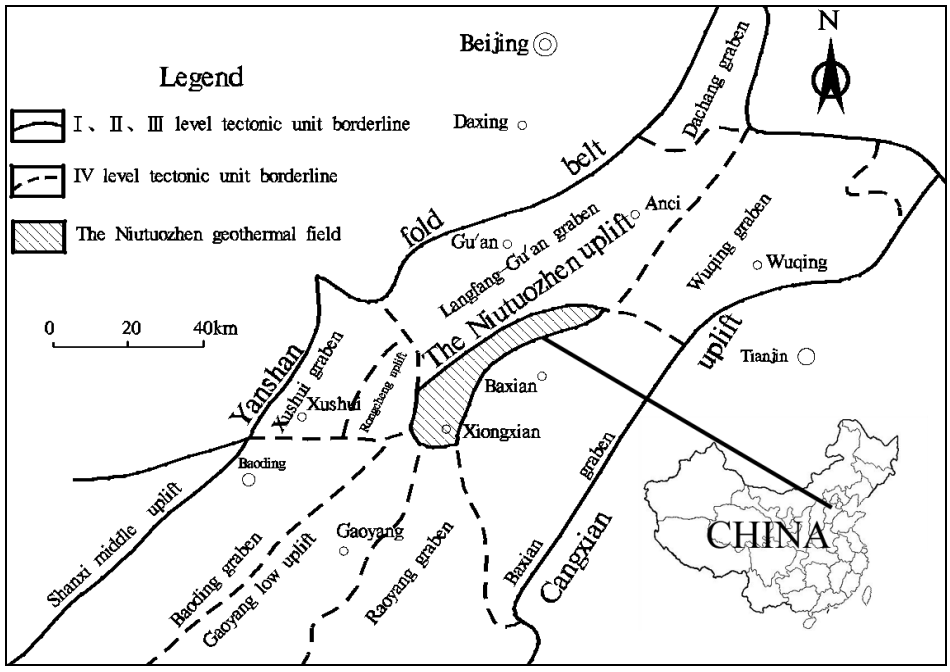

FIGURE 1: Tectonic location of the Niutuozhen geothermal field in North China

Geothermal Group, 1983; Zhou, 1987; Zhou et al., 1989; Ma, 1990 and Liu et al., 2005). For more than 30 years, geothermal water, ranging in temperature between 60 and 85°C, has mostly been used for resident space heating, greenhouse horticulture, swimming pools, balneology and general industry in the towns of Xiongxian and Gu'an. As a result of drastically increased exploitation, proper management of the field is currently needed to guarantee long time sustainable development of the geothermal resources.

Numerical modelling is a quantitative method to explain some elements of mechanism and formation conditions of a geothermal system and make predictions of geothermal field performance based on the simulated response of the geothermal system to its production history. Successful management and sustainable development have been achieved in many geothermal fields all over the world by using a numerical geothermal model (Wu and Pruess K., 1998).

AQUA3D was used to build a 3D numerical model of the Niutuozhen geothermal field. AQUA3D is a software package developed by Vatnaskil Consulting Engineers to solve three-dimensional groundwater flow and transport problems using the Galerkin finite element method. In brief, AQUA3D solves the equations describing groundwater flow and transport for both homogeneous, isotropic aquifers and inhomogeneous, anisotropic aquifers. The programme also solves the transient transport equations for the movement of contaminants, heat with convection, decay, adsorption and velocity dependent dispersion (Vatnaskil, 1998). It has been used to build models of a few low-temperature geothermal fields in China (Hu, 1994).

Seven layers were determined according to the various permeability of the formation. The dolomite of the Jixian system with strong carst erosion and the sandstone of Neogene with high porosity are the main geothermal reservoirs and cover the entire geothermal field; other layers, however, exist only in the northeast. All the boundaries of layers 1 and 2 are set as flow boundaries. From layer 3 to layer 7, no-flow boundaries are set in the west, south and east due to four water-resisting faults. The northern boundary is set as a flow boundary because the layers extend continuously to the north.

In order to maintain sustainable development of geothermal energy in the long run, predictions of water level change and heat transport, corresponding to specific production and reinjection rates over the next 20 years, i.e. from 2010 to 2030, were made by the flow and transport model. This can provide valuable information for geothermal field management.

2. THE AQUA3D DISTRIBUTED PARAMETER MODEL

AQUA3D solves three-dimensional groundwater flow and transport equations. In the flow equation, the top layer can be treated as confined or unconfined. In the case of an unconfined aquifer, the equations become nonlinear and are then solved by iteration. The aquifer can be divided vertically into as many layers as necessary, and these layers can be separated by semi-permeable layers. The transport equation can be solved both for the transport of contaminants and heat. The user decides which one he wants to solve by proper selection of the input parameters.

2.1 Flow model

The three-dimensional movement of groundwater with constant density may be described by the following partial differential equation:

$$\frac{\partial}{\partial x}\left(K_{xx}\frac{\partial h}{\partial x}\right)+\frac{\partial}{\partial y}\left(K_{yy}\frac{\partial h}{\partial y}\right)+\frac{\partial}{\partial z}\left(K_{zz}\frac{\partial h}{\partial z}\right)=S_s\frac{\partial h}{\partial t}-Q \tag{1}$$

where K_{xx}, K_{yy}, K_{zz} = Hydraulic conductivities along the principal axes (m/s);
h = Piezometric head (m);
Q = Volumetric flux per unit volume ($m^3/s/m^3$);
S_s = Specific storativity (m^{-1}); and
t = Time (s).

In the above equation it is assumed that the principal axes are in horizontal and vertical planes. The above equation applies to a local coordinate system within each element, so anisotropy can vary from element to element. The aquifer is now discretised into as many layers as necessary and the above equation is integrated across each layer. The resulting equations are given below for n layers counted from top to bottom.

Top layer:

$$\frac{\partial}{\partial x}\left(T_{xx}\frac{\partial h_1}{\partial x}\right)+\frac{\partial}{\partial y}\left(T_{yy}\frac{\partial h_1}{\partial y}\right)+R+\gamma_2\left(h_2-h_1\right)+Q=S\frac{\partial h_1}{\partial t}+S_y \tag{2}$$

Layer i:

$$\frac{\partial}{\partial x}\left(T_{xx1}\frac{\partial h_i}{\partial x}\right)+\frac{\partial}{\partial y}\left(t_1\frac{\partial h_i}{\partial y}\right)+\gamma_i\left(h_{i-1}-h_i\right)+\gamma_{i+1}\left(h_{i+1}-h_i\right)+Q=S\frac{\partial h_i}{\partial t} \tag{3}$$

Bottom layer:

$$\frac{\partial}{\partial x}\left(T_{xx}\frac{\partial h_n}{\partial x}\right)+\frac{\partial}{\partial y}\left(T_{yy}\frac{\partial h_n}{\partial y}\right)+\gamma_n\left(h_{n-1}-h_n\right)+Q=S\frac{\partial h_n}{\partial t} \tag{4}$$

where γ_i = The average vertical conductance, defined as the vertical conductance of layer i.

The transmissivity or horizontal conductance is defined as follows:

$T_{xx} = K_{xx} \times$ Saturated thickness of layer;
$T_{yy} = K_{yy} \times$ Saturated thickness of layer.

The storage coefficient in the top layer is defined as:

$S = S_s \times$ Saturated thickness of layer + S_y;

and in layer *i:*

$S = S_s \times$ Saturated thickness of layer.

Here, both the vertical permeability in each layer as well as the vertical permeability in possible semi-permeable layers between the layers has taken into account. The following definitions apply for the equations above:

T_{xx}, T_{yy} = The transmissivities along the principal axes in each layer (m^2/s);
K_{xx} ,K_{yy} = Hydraulic conductivities along the principal axes in each layer(m/s);
S_s = Specific storativity in each layer (m^{-1});
h_i = Piezometric head in layer i (m);
R = Infiltration rater (mm/year);
Q = Pumping/injection rate in each layer (m^3/s); and
S_y = Specific yield (m^{-1}).

The following three kinds of boundary conditions are allowed in each layer:

1) Dirichlet boundary condition;
2) Von Neumann boundary condition; and
3) Cauchy boundary condition.

In the Dirichlet boundary condition the groundwater level, the piezometric head or the potential function is prescribed at the boundary as a function of time. In the Von Neumann boundary condition, the flow at the boundary is prescribed. Any given flow at a boundary can be modelled by defining source nodes (recharge of pumping) at the no-flow boundary nodes. The Cauchy boundary condition is a head-dependant condition. The flow rate is related to both the normal boundary derivative and the head.

2.2 Heat transport model

The three-dimensional transport of mass/heat in groundwater may be described by the following partial differential equation:

$$\frac{\partial}{\partial x}\left(D_{xx}\frac{\partial c}{\partial x}\right)+\frac{\partial}{\partial y}\left(D_{yy}\frac{\partial c}{\partial y}\right)+\frac{\partial}{\partial z}\left(D_{zz}\frac{\partial c}{\partial z}\right)+Q(c_w-c)-\left(V_x\frac{\partial c}{\partial x}+V_y\frac{\partial c}{\partial y}+V_z\frac{\partial c}{\partial z}\right) = \varphi R_d\frac{\partial c}{\partial t}+\varphi R_d\lambda c \tag{5}$$

The above equation applies to a local coordinate system within each element, having the main axis along the flow direction.

It has been assumed that for dispersive transport, vertical flow velocities are less than the horizontal flow velocities. The dispersion coefficients, D_{xx}, D_{yy} and D_{zz} are then defined by:

$$\varphi D_{xx}=\alpha_L V^n+D_m\varphi \tag{6}$$

$$\varphi D_{yy}=\alpha_T V^n+D_m\varphi \tag{7}$$

$$\varphi D_{zz}=\alpha_T V^n+D_m\varphi \tag{8}$$

The retardation coefficients R_d are given by:

$$R_d=1+\beta(1-\varphi)\rho_s/(\varphi\rho_l) \tag{9}$$

where β = The retardation constant.

The retardation constant for mass transport is defined as:

$$\beta = K_d \rho_l \tag{10}$$

and for heat transport as:

$$\beta = C_s / C_l \tag{11}$$

The following definitions apply for the equations above:

c = Solute concentration/temperature;
V_x, V_y, V_z = Velocity vectors taken from the solution of the flow problem (m/);
α_L = Longitudinal dispersivity (m);
α_T = Transversal dispersivity (m);
V = Velocity (m/s);
D_m = Molecular difussivity (m^2/s);
φ = Porosity;
c_w = Concentration/temperature of injection water;
Q = Pumping/injection rate (m^3/s);
λ = Exponential decay constant (s^{-1});
K_d = Distribution coefficient;
ρ_l = Density of the liquid (kg/m^3);
ρ_s = Density of the porous medium (kg/m^3);
C_l = Specific heat capacity of the liquid(J/kg • °C) and
C_s = Specific heat capacity of the porous medium (J/kg • °C).

Equation 5 is now integrated vertically across each layer. The results are given below for n layers counted from top to bottom.

Top layer:

$$\begin{aligned}&\frac{\partial}{\partial x}\left(\varphi b_1 D_{xx}\frac{\partial c_1}{\partial x}\right)+\frac{\partial}{\partial y}\left(\varphi b_1 D_{yy}\frac{\partial c_1}{\partial y}\right)-\left(V_x b_1\frac{\partial c_1}{\partial x}+V_y b_1\frac{\partial c_1}{\partial y}\right)\\&=\varphi b_1 R_d\frac{\partial c_1}{\partial t}+\varphi b_1 R_d\lambda c_1-(c_0-c_1)R-Q(c_w-c_1)-\gamma_2(h_2-h_1)(c_{1,2}-c_1)-\delta_2(c_2-c_1)\end{aligned} \tag{12}$$

Layer i:

$$\begin{aligned}&\frac{\partial}{\partial x}\left(\varphi b_i D_{xx}\frac{\partial c_i}{\partial x}\right)+\frac{\partial}{\partial y}\left(\varphi b_i D_{yy}\frac{\partial c_i}{\partial y}\right)-\left(V_x b_i\frac{\partial c_i}{\partial x}+V_y b_i\frac{\partial c_i}{\partial y}\right)\\&=\varphi b_i R_d\frac{\partial c_i}{\partial t}+\varphi b_i R_d\lambda c_i-Q(c_w-c_i)-\gamma_i(h_{i-1}-h_i)(c_{i,i-1}-c_i)-\gamma_{i+1}(h_{i+1}-h_i)(c_{i,i+1}-c_i)\\&-\delta_i(c_{i-1}-c_i)-\delta_{i+1}(c_{i+1}-c_i)\end{aligned} \tag{13}$$

Bottom layer:

$$\begin{aligned}&\frac{\partial}{\partial x}\left(\varphi b_n D_{xx}\frac{\partial c_n}{\partial x}\right)+\frac{\partial}{\partial y}\left(\varphi b_n D_{yy}\frac{\partial c_n}{\partial y}\right)-\left(V_x b_n\frac{\partial c_n}{\partial x}+V_y b_n\frac{\partial c_n}{\partial y}\right)\\&=\varphi b_n R_d\frac{\partial c_n}{\partial t}+\varphi b_n R_d\lambda c_n-Q(c_w-c_n)-\gamma_n(h_{n-1}-h_n)(c_{n,n-1}-c_n)-\gamma_{n+1}(h_{n+1}-h_n)(c_{n,n+1}-c_n)\\&-\delta_n(c_{n-1}-c_n)-\delta_{n+1}(c_{n+1}-c_n)\end{aligned} \tag{14}$$

where b_i is the saturated thickness of each layer; and:

$$c_{i,i-1} = \begin{bmatrix} c_i & \text{for outflow} \\ c_{i-1} & \text{for inflow} \end{bmatrix} \tag{15}$$

The average vertical dispersion coefficient, δ_i is defined when we have taken into account both vertical dispersion in each layer as well as vertical dispersion in possible semi-permeable layers between the layers.

The following definitions apply for the equations above:

D_{xx}, D_{yy}, D_{zz} = Dispersion coefficents along the principal axes in each layer (m^2/s);
D_z = Vertical dispersion coefficient in a semi-permeable layer between layers (m/s); and
c_i = Concentration/temperature in layer i.

The following two types of boundary conditions are allowed in each layer.

1) Dirichlet boundary condition; and
2) Von Neumann boundary condition.

In the Dirichlet boundary condition the concentration or temperature is specified at the boundary. In the Von Neumann boundary condition the concentration gradient or the temperature gradient is set to zero, indicating only convective transport of mass or heat through the boundary.

3. MODELLING OF THE NIUTUOZHEN GEOTHERMAL FIELD

A three-dimensional numerical model was built to simulate the main reservoirs, the Jixian system and the Neogene reservoirs, of the Niutuozhen geothermal system. Prediction on water level change according to the specified production was made by a flow model and heat field change as a response to the reinjection.

3.1 Geological background

The Niutuozhen geothermal system is located in the Niutuozhen uplift zone which is situated in the northern part of the Jizhong graben in the North China basin. The basin began developing by the vertical movement of crust before the Late Triassic period, followed by mountain building from Jurassic to early Tertiary and subsidence during Late Miocene. The NE-SW oriented uplifts and grabens were formed alternately from west to east (Figure 2) along the tectonic line. The Niutuozhen uplift is constrained by the revived Niudong fault, Niunan fault, Rongcheng fault and Daxing fault which resulted from folding movement from the Late Jurassic to the Cretaceous, formed during the Himalayan movement. By the Late Oligocene, the Niutuozhen uplift still continuously moved up to surface to be eroded before it became mature. The Neogene and Quaternary sedimentary deposited over the entire Niutuozhen uplift by the Late Miocene.

The Niudong normal fault striking 60 km northeast with 40°E dip is the control boundary between the Niutuozhen uplift and the Baxian graben. The vertical and horizontal slips are generally 7000 m and 1100 m, respectively. The Niunan normal fault striking 23 km west dipping 45°S is the southern boundary of the Niutuozhen uplift. The vertical slip of the fault is from 1200 to 3200 m. The horizontal slip is between 1000 and 2500 m. The Daxing normal fault striking 45 km northeast with a southeasterly dip is the northwest boundary of the Niutuozhen uplift. The vertical slip is between

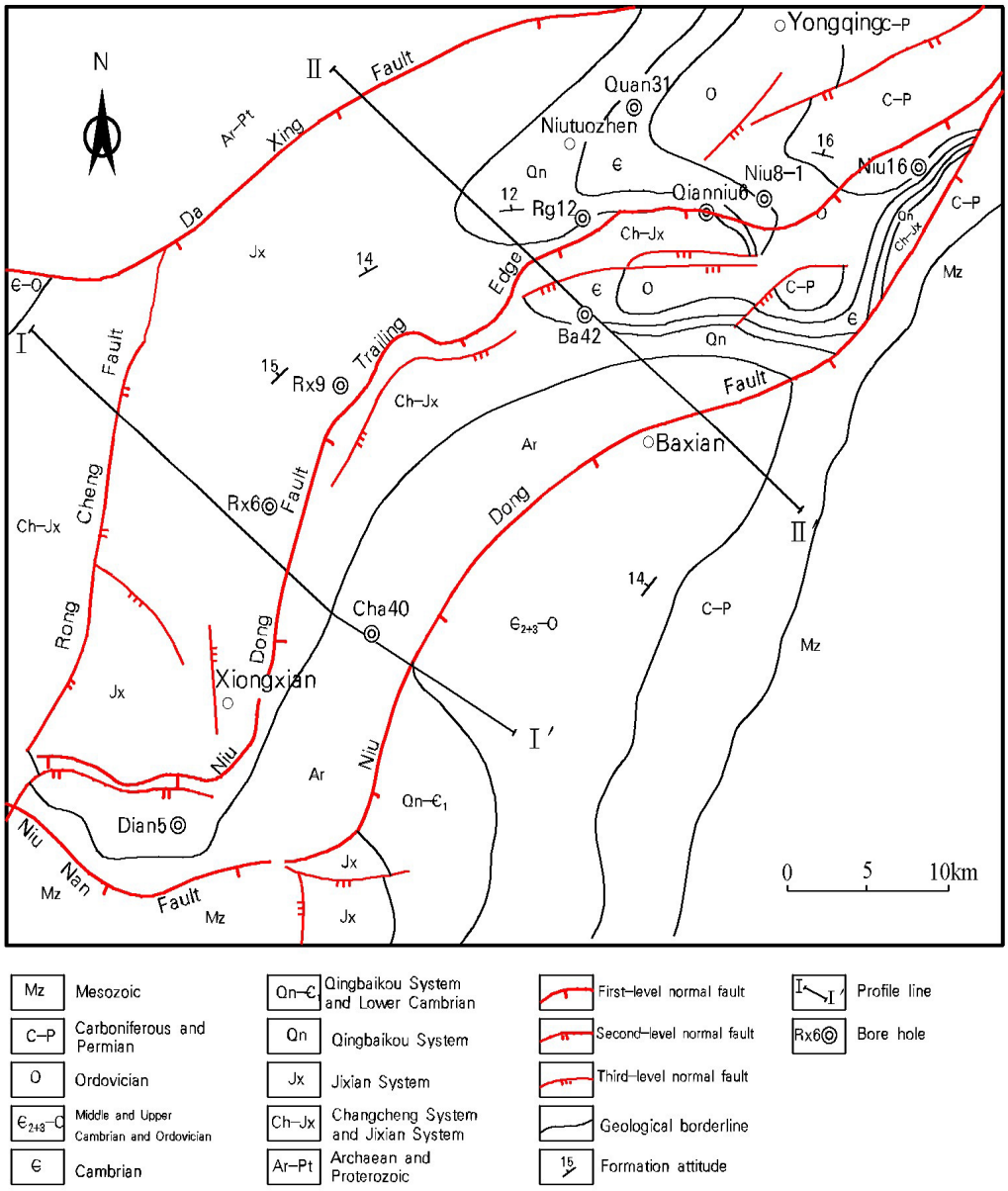

FIGURE 2: Regional geological map of Niutuozhen uplift

200 and 300 m. The Rongcheng normal fault striking 30 km north and dipping 45°E is the western boundary of the Niutuozhen uplift. The vertical slip is 3000 m and horizontal slip is between 1000 and 3000 m as shown in Figures 3 and 4.

Gneiss, granulites and crystal metamorphic rocks of the Archaean were mostly found in the northwest and eastern slopes of the Niutuozhen uplift. A sequence of clastic rocks, mudstone-carbonatite-mudstone and clastic rocks of the Changcheng system, Jixian system and Qingbaikou system was deposited in the middle and south of the region as a result of regression and progression. Carbonite and mudstone of the Cambrian and Ordovician only occurred in the northeast. The Carboniferous and Permian in the northeast are composed of marine and continental mudstone with alternating facies, thin limestone and some continental facies clastic rocks. Mudstone and sandstone of the Palaeogene were only deposited in the western and eastern grabens surrounding the Niutuozhen uplift. The Neogene formations containing sandstone and mudstone encompass the entire region, which is covered by the Deluvial and alluvial materials of the Quaternary (Table 1).

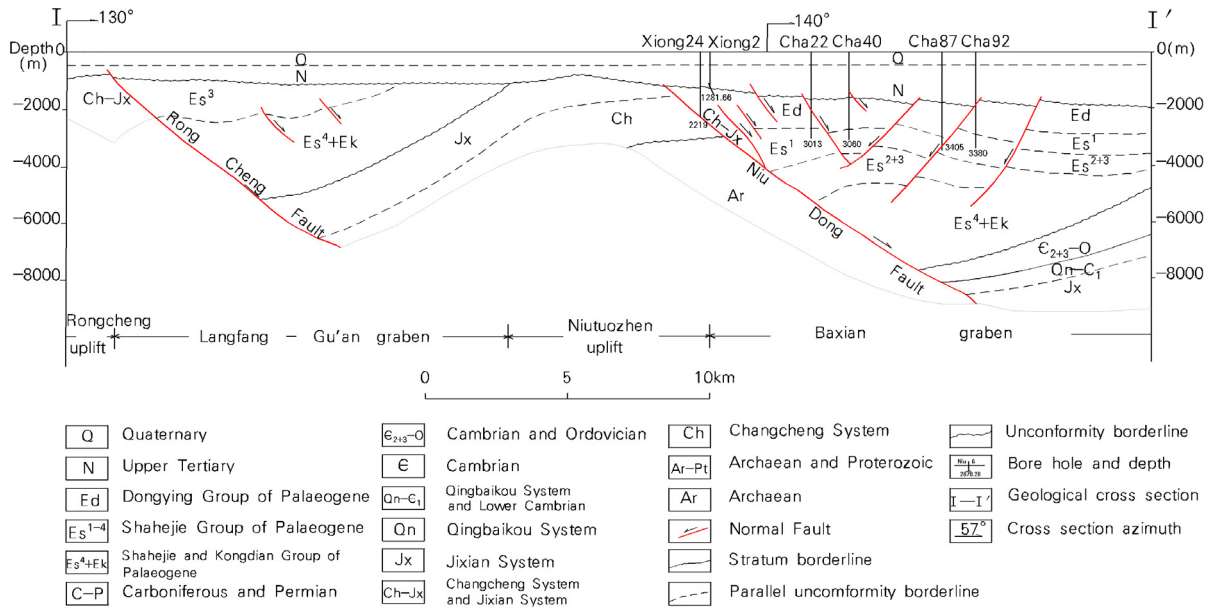

FIGURE 3: Geological cross-section I-I' of the Niutuozhen geothermal field; location is shown in Figure 2

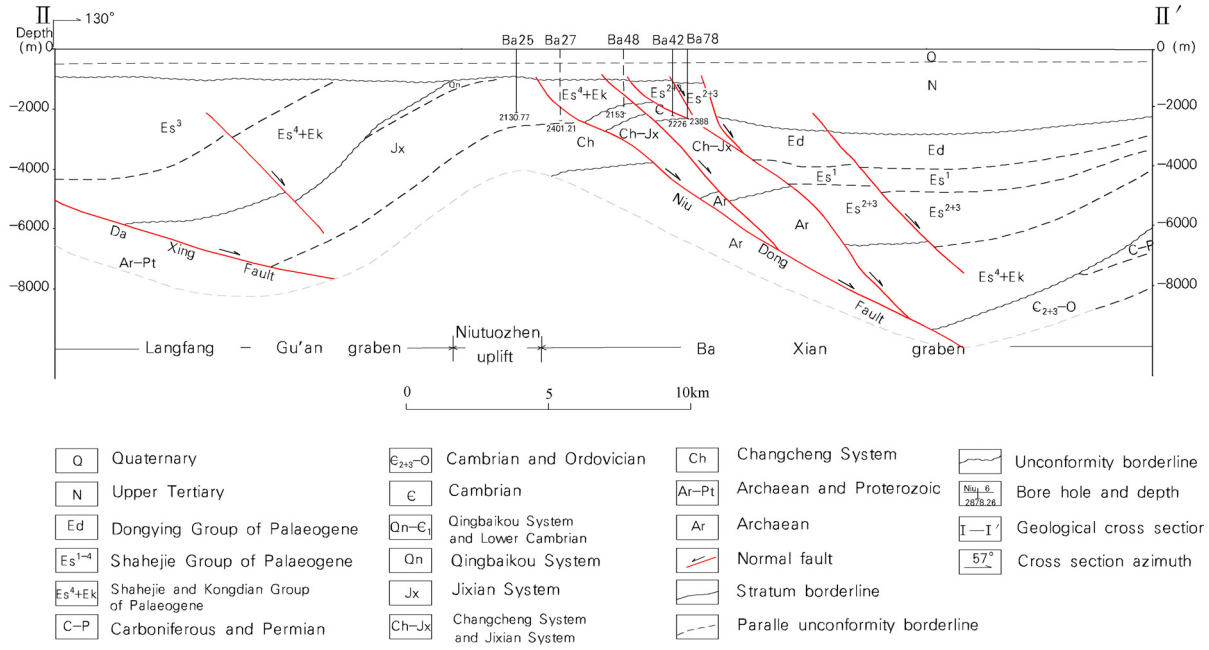

FIGURE 4: Geological cross-section II-II' of the Niutuozhen geothermal field; location is shown in Figure 2

TABLE 1: Stratum of Niutuozhen uplift

Formation	Thickness (m)	Location	Lithology
Archaean	>10000	Limbs of Niutuozhen uplift	Granulites & crystal metamorphoric rocks
Changcheng	372-1811	Upper wall of Niudong & Rongcheng faults	Clastic rocks and mudstone
Jixian	1045-3106	Middle, west and south of Niutuozhen uplift	Dolomite and mudstone
Qingbaikou	0-359	Middle and east of Niutuozhen uplift	Clastic rocks and mudstone
Cambrian	353-780	Middle and east of Niutuozhen uplift	Carbontite and mudstone
Ordovician	540-933	Middle and east of Niutuozhen uplift	Carbontite and mudstone
Carboniferous	100-220	Northeast of Niutuozhen uplift	Mudstone and thin limestone
Permian	460-1032	Northeast of Niutuozhen uplift	Mudstone and thin limestone
Palaeogene	0-8000	Grabens around Niutuozhen uplift	Mudstone and sandstone
Neogene	114-1800	Entire area	Sandstone and mudstone
Quaternary	380-470	Entire area	Deluvial and alluvial materials

3.2 Thermal field

The tectonic framework of the uplifts and grabens in this region is reflected by the thermal gradient of the cap rock as shown in Figure 5. The caprock's geothermal gradient in the Niutuozhen uplift is more than 3.0°C/100 m, and 8°C/100 m measured in the axis of the uplift. The geothermal gradient relates well with the caprock's thickness; a higher gradient corresponds to smaller thickness, and a lower gradient corresponds to greater thickness (Chen, 1988).

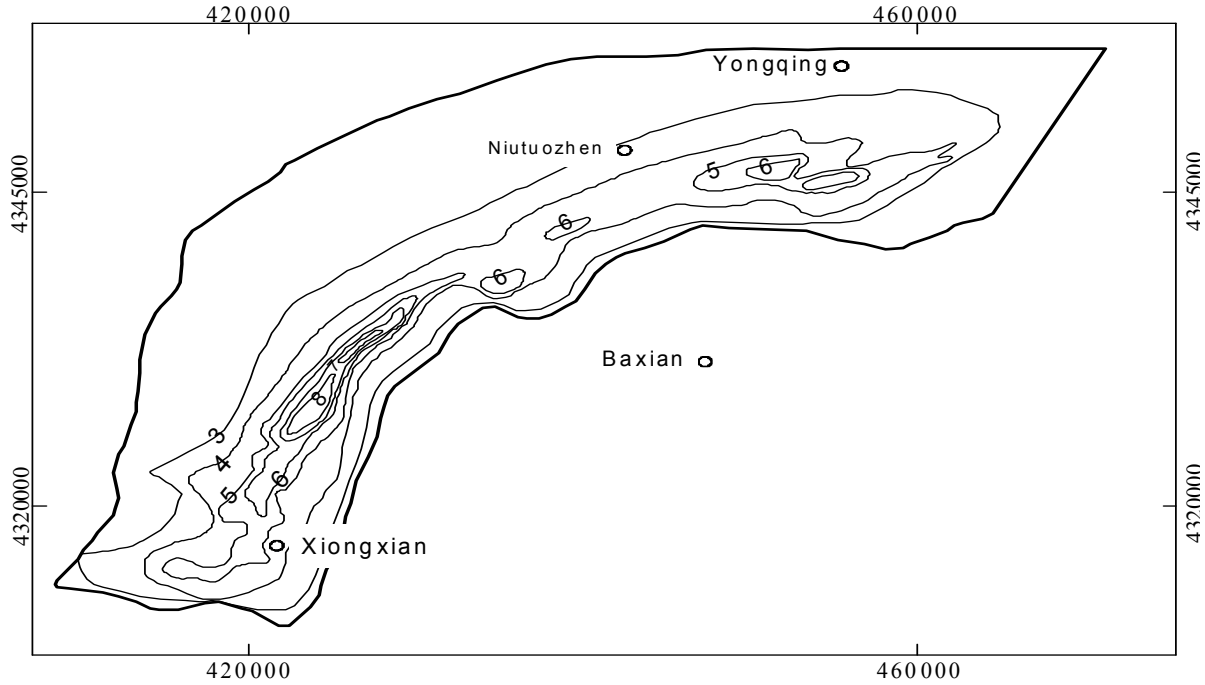

FIGURE 5: Thermal gradient (°C/100 m) in the caprock of the Niutuozhen geothermal field

3.3 Conceptual reservoir model

The conceptual model is three-dimensional; including an area of 1000 km^2 within the Niutuozhen uplift controlled by four faults, and extends to a depth of 8 km, at the bottom of the lowest reservoir. For the numerical simulations, the rocks were divided into 7 vertical layers, corresponding in composition and depth to the major rock units identified by previous geological studies (Chen et al., 1982; Geothermal Group, 1983; Chen et al., 1985; Zhou, 1987; Zhou et al., 1989; Ma et al., 1990 and Liu et al., 2005).

Of these, the upper layer, which is 700 m thick, corresponds to the permeable sandstone and impermeable mudstone of the Neogene, which is one of the main reservoirs of the Niutuozhen geothermal field. Layer 2 is 0 to 7000 m thick, corresponding to the impermeable mudstone of Palaeogene. Layer 3 includes impermeable mudstone and clastic rocks of Carboniferous and Permian. Permeable limestone with strong carst of Cambrian and Ordovician age is determined as Layer 4. Layer 5 is the mudstone of the Qingbaikou system. The dolomite with strong carst of the Jixian system and part of the Changcheng system were divided into two layers, 6 and 7. These layers represent the reservoirs with the largest volume and production capacity in the Niutuozhen geothermal field. The reason for separating layers 6 and 7 was because layer 6 has a higher permeability due to a higher occurrence of carst than layer 7. Impermeable mudstone and Archaean impermeable gneiss is at the bottom of the model as shown in Figure 6.

For layers 1 and 2, all boundaries were set as flow boundaries, because layer 1 extends in all directions without limits. For layers 3 to 7, the eastern, southern, and western boundaries were set as closed boundaries according to the water resistant faults developed along the boundaries (Ma et al., 1990). The northern boundary was defined as a flow boundary corresponding to the tectonic settings (Qi et al., 2004 and Zhou, 1987).

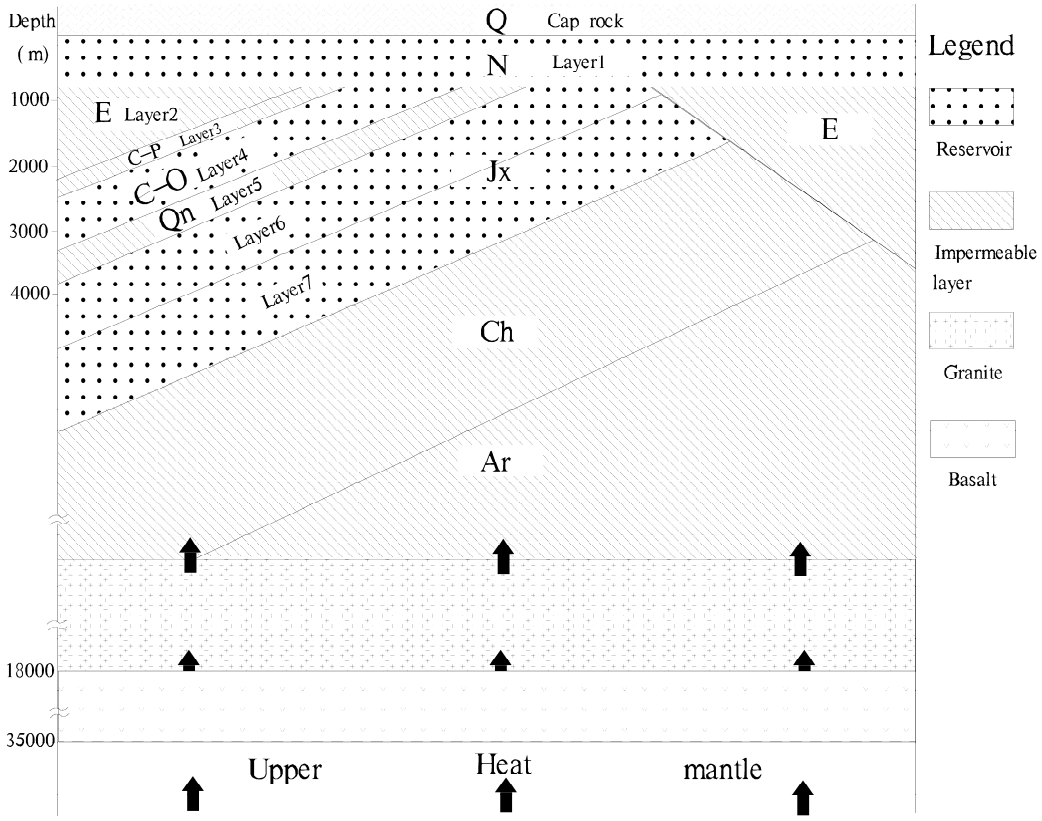

FIGURE 6: The conceptual model of the Niutuozhen geothermal system

3.4 Exploitation history

Beginning in the 1970s and extending to 1986, the geothermal resources were initially used for greenhouse heating, hatching, fish farming, industry drying and resident space heating on a small scale. After 1986, space heating became the major demand for geothermal water, resulting in a drastic increase in geothermal development and production (Table 2). Xiongxian in the southwest and Gu'an in the northeast are the two towns that are taking advantage of clean geothermal energy instead of coal, especially in resident space heating, to build *no-smoke towns* in North China, widely supported by the local people and government.

TABLE 2: Annual production of the Jixian system reservoir in the Niutuozhen geothermal field

Year	Production (10^4m^3)	Year	Production (10^4m^3)	Year	Production (10^4m^3)	Year	Production (10^4m^3)
1973	10	1982	26	1991	91	2000	149
1974	6	1983	26	1992	99	2001	161
1975	6	1984	26	1993	110	2002	160
1976	10	1985	26	1994	123	2003	149
1977	26	1986	41	1995	136	2004	153
1978	26	1987	47	1996	136	2005	166
1979	26	1988	52	1997	136	2006	176
1980	26	1989	79	1998	140	2007	258
1981	26	1990	91	1999	153	2008	292

The Jixian system reservoir is the main reservoir because of its high production capacity and relatively high temperature compared to the upper Neogene sandstone reservoir. As of 2009, 41 wells had been drilled for production, four into the Neogene reservoir and 37 into the Jixian system. Of these, three wells are currently operational in the Neogene system and 32 wells in the Jixian system (Figure 7).

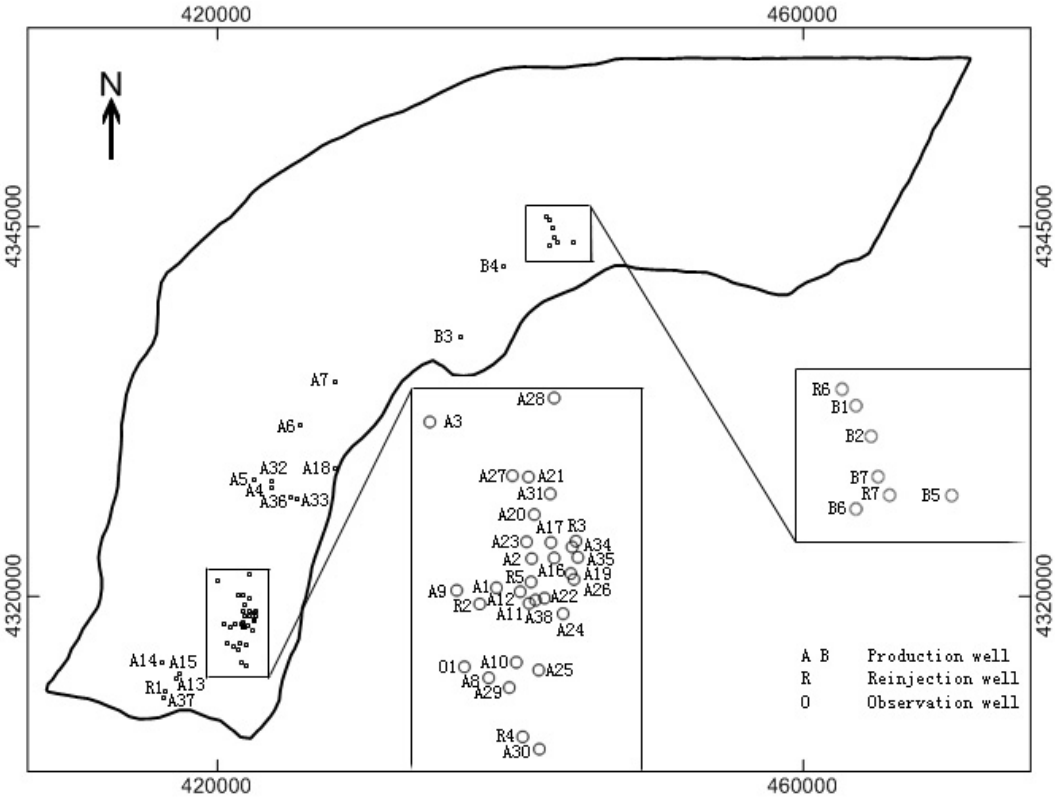

FIGURE 7: Location of wells in the Niutuozhen geothermal field

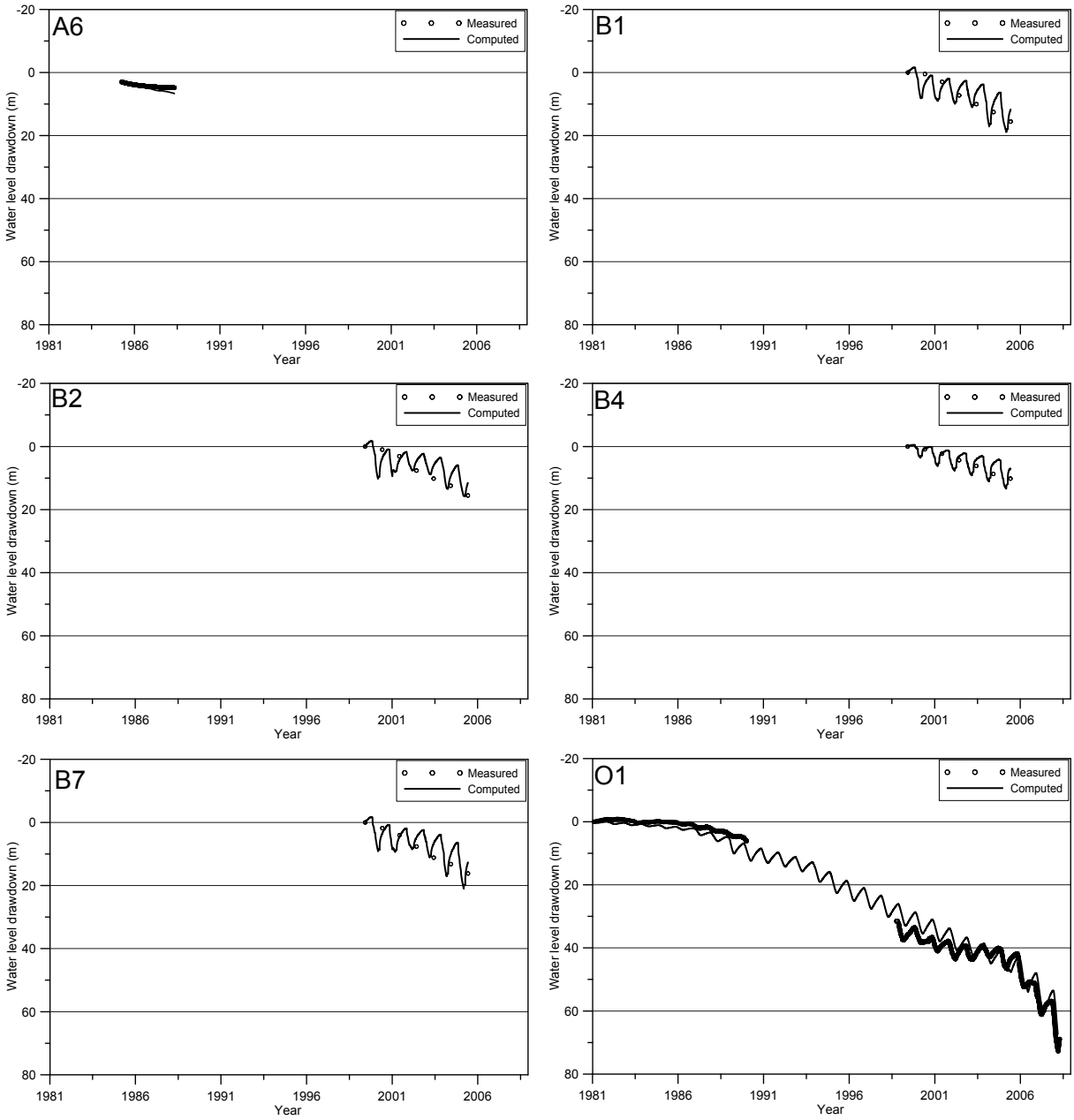

FIGURE 8: Comparison of computed and measured drawdown histories in six wells

3.5 Calibration of reservoir parameters using the AQUA3D model

An initial set of parameters used in the model for simulation was estimated from values calculated by Zhou et al. (1989), Ma et al. (1990) and Liu et al. (2005) and from the properties of different rock formations. The boundary conditions were set as described by the conceptual model. Initial conditions were defined from the natural state of the system prior to any production. A computed match to the measured water level drawdown was used to obtain the best parameters to define the reservoir. The measured and computed drawdown histories in six wells, one monitoring well (O1) and five productions wells (A6, B1, B2, B4 and B7), are depicted in Figure 8. Well A6, representing the Neogene reservoir, exhibited a slow but straight drawdown during its production history. The simulated results show the same drawdown trend and rate. Wells B1, B2, B4 and B7, four representative wells in the Jixian system in the north of the field, show continuous drawdown. The simulated results display the same drawdown but with fluctuations in different seasons because the production rate in winter is more than during other seasons. Water levels in well B1, B2, B4 and B7

measured in June from 2000 to 2006 are between the peak and valley of the computed drawdown because of the water level recovery after the space heating season. The water level in well A6 was measured from 1986 to 1989. Daily water level data is available for well O1 from 1981 to 2009, except for a break from 1990 to 1999. Well O1, a monitoring well in the south of the field, shows a sharp and continuous drawdown, matched by the simulated results. The measured and the computed drawdown in these wells show the same fluctuation due to different production rates.

The mudstones in layers 2, 3 and 5 are impermeable and assigned with a rather lower permeability. All the layers are divided into several areas with different permeability as the permeability in the axis of Niutuozhen uplift is generally larger than in the area which deviates from the axis. Given that there is no production from layer 4 and no monitoring wells in layers 4 and 7, the water level drawdown was fitted to data from 6 wells, one in layer 1 and five in layer 6. A reliable flow model was built after an acceptable match had been obtained between calculated and measured values through calibration (Figures 9 and 10; Table 3).

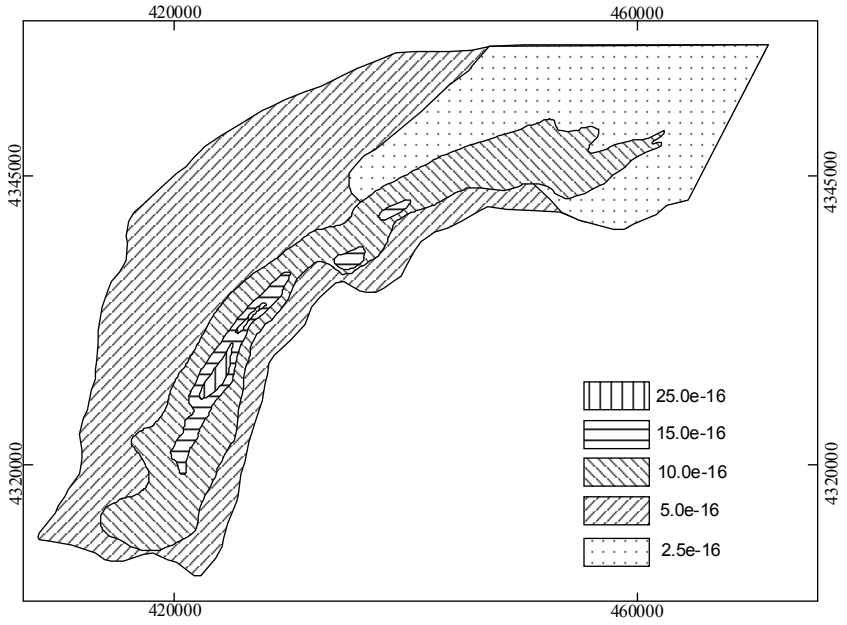

FIGURE 9: Permeability distribution of layer 6 of the Niutuozhen geothermal field (m^2)

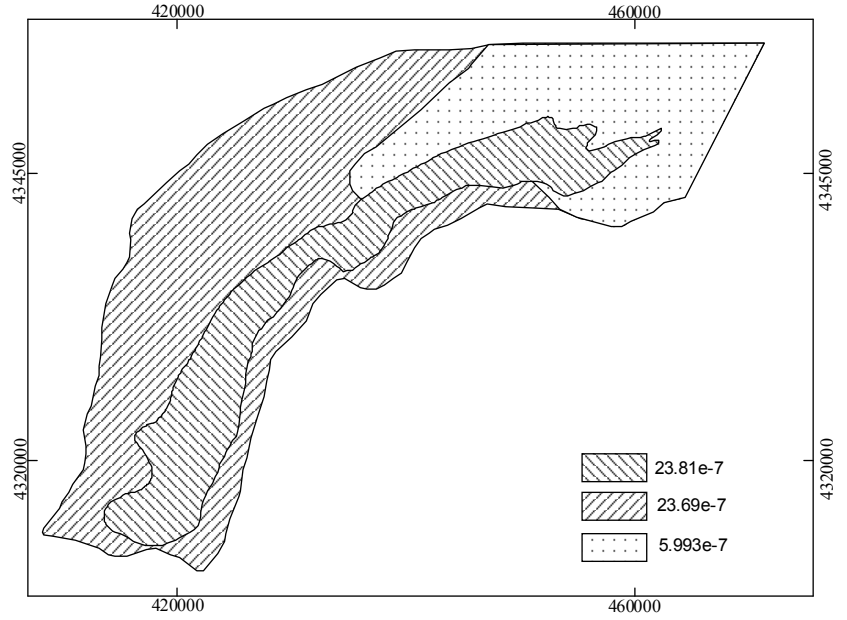

FIGURE 10: Specific storativity distribution of layer 6 of the Niutuozhen geothermal field (m^{-1})

TABLE 3: Reservoir parameters for the layers of the model

Layer	1	2	3	4	5	6	7
Permeability (10^{-16} m^2)	5	0.003	0.0001	5-25	0.0001	2.5-25	0.25-2.5
Specific storativity (10^{-7}m^{-1})	285.9	0.2486	1×10^{-12}	5.993-23.81	1×10^{-12}	5.993-23.81	0.5993-2.381

4. RESERVOIR PERFORMANCE PREDICTION

With increasing concern for environmental protection and energy demand, geothermal development in China is on the rise. The Chinese government is investing heavily in geothermal energy, and reasonable geothermal reservoir management along with sustainable exploitation are indispensable. Reservoir pressure drawdown and reservoir cooling resulting from increased production and reinjection with lower temperature water are two significant problems. Flow and transport models are used for predicting reservoir response to future geothermal energy exploitation.

In order to predict the reservoir response according to different production and reinjection scenarios for the next 20 years, from 2010 to 2030 (Table 4), six scenarios were proposed for layer 6.

TABLE 4: Proposed production and reinjection in Niutuozhen geothermal field

Scenario	Production rate (l/s)	Production increment (%)	Reinjection rate (%)	Reinjection temperature (°C)
I	108	0	0	
II	108	0	20	40
III	129	20	0	
IV	129	20	50	40
V	162	50	0	
VI	162	50	50	40

Note: 1) Production increment is the percent increase from the current production (2009);
2) The reinjection rate is shown as a percentage of the total production.

The main assumptions used in model were:

1) No new production wells will be drilled during the prediction period; therefore, the increased production is added to the current production wells. The distance between the current production wells is so close that the increased production from the current production wells will cause the same drawdown as in new production wells.
2) Given that currently there is more production in the south than in the north, five unused production wells were set as reinjection wells in the south and two in the north.
3) The reinjection rate is based on the local production rate, which is higher in the southern area (wells denoted by A) than in the northern area (wells denoted by B).
4) Twenty percent reinjection was assumed for the prediction, based on current production. The reinjection rate was increased to fifty percent, taking into account the reinjection capacity of the reservoir and the cooling potential.
5) The temperature of the geothermal water after use is approximately 40°C currently and so set as the temperature of the reinjected water.

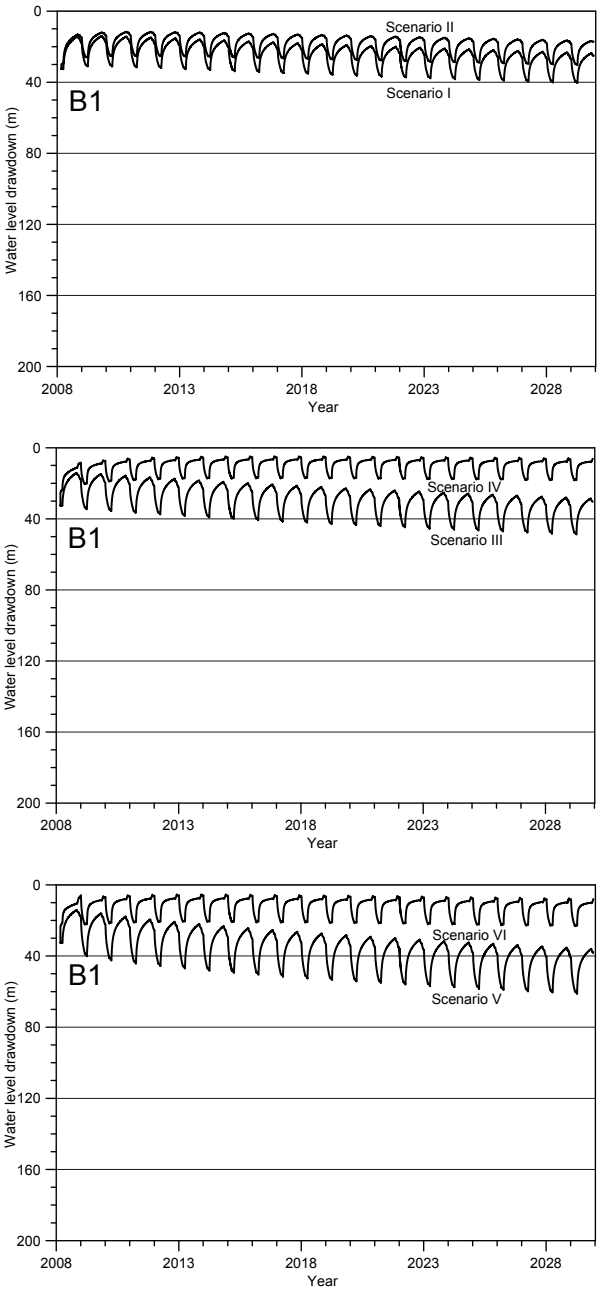

FIGURE 11: Predicted drawdown in well B1 for different scenarios

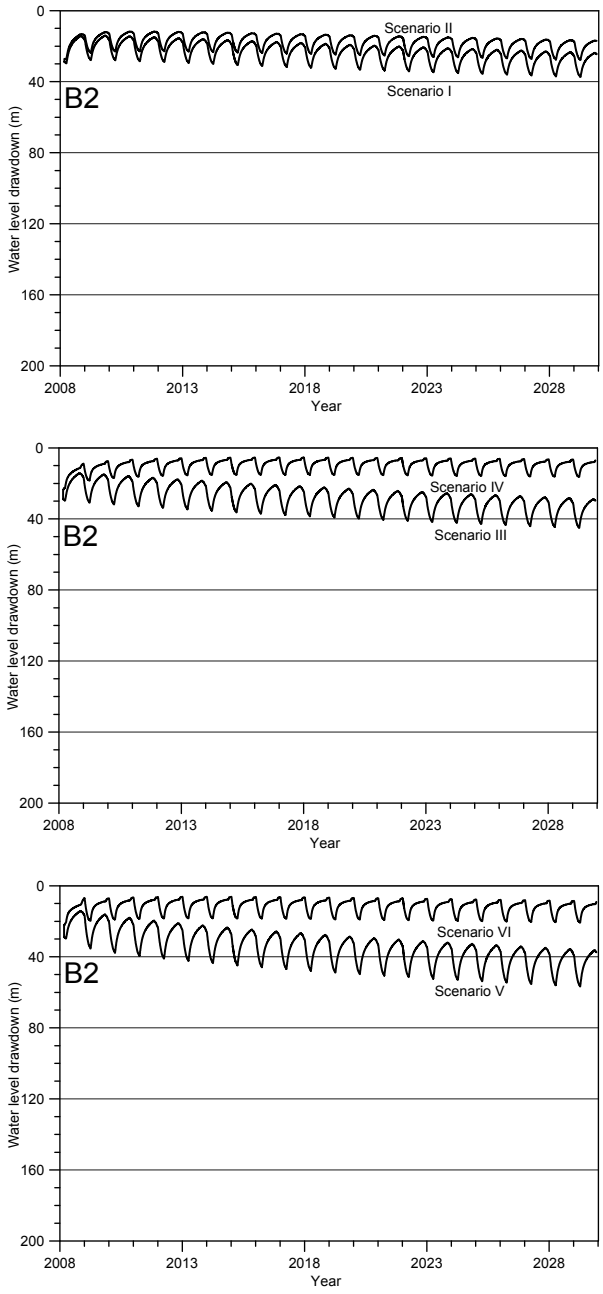

FIGURE 12: Predicted drawdown in well B2 for different scenarios

4.1 Predicted pressure change

4.1.1 Predicted pressure change in wells

Figures 11, 12, 13 and 14 show the predicted drawdown according to the six scenarios in wells B1, B2, B4 and B7, located in the northern part of the field. Corresponding to a proposed production of 108, 129 and 162 l/s without reinjection, the drawdown was predicted to increase from 10, 20 or 30 m at the end of 2030 in wells B1, B2 and B4, respectively. More drawdown was predicted in well B7 (Figure 14) because of possibly higher production.

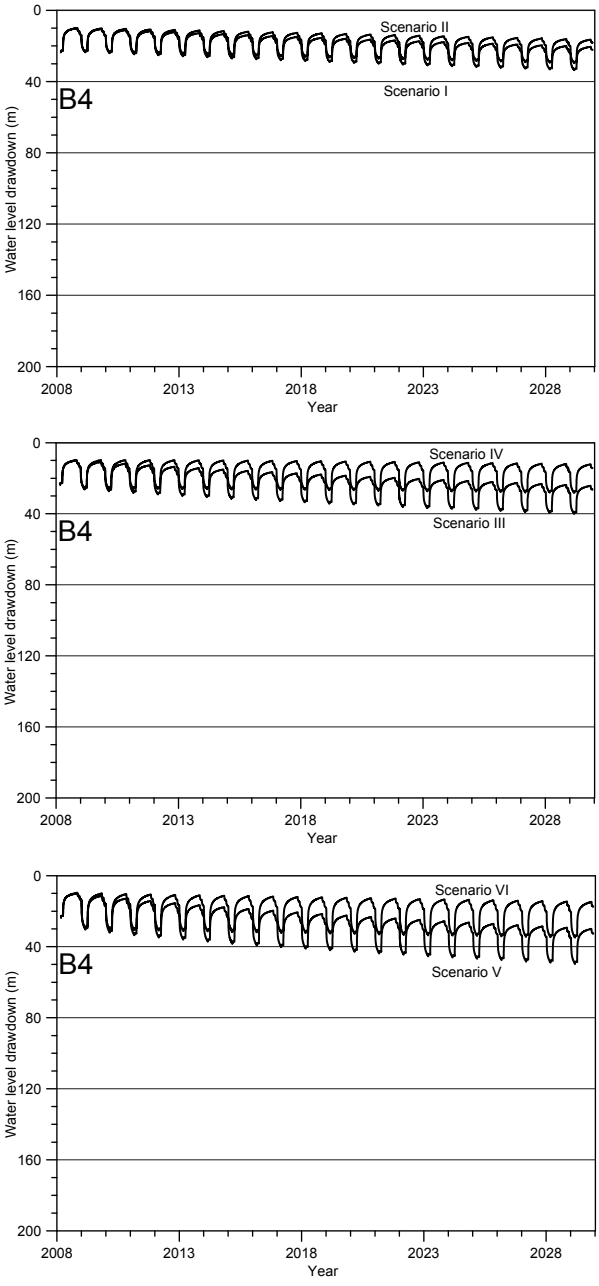

FIGURE 13: Predicted drawdown in well B4 for different scenarios

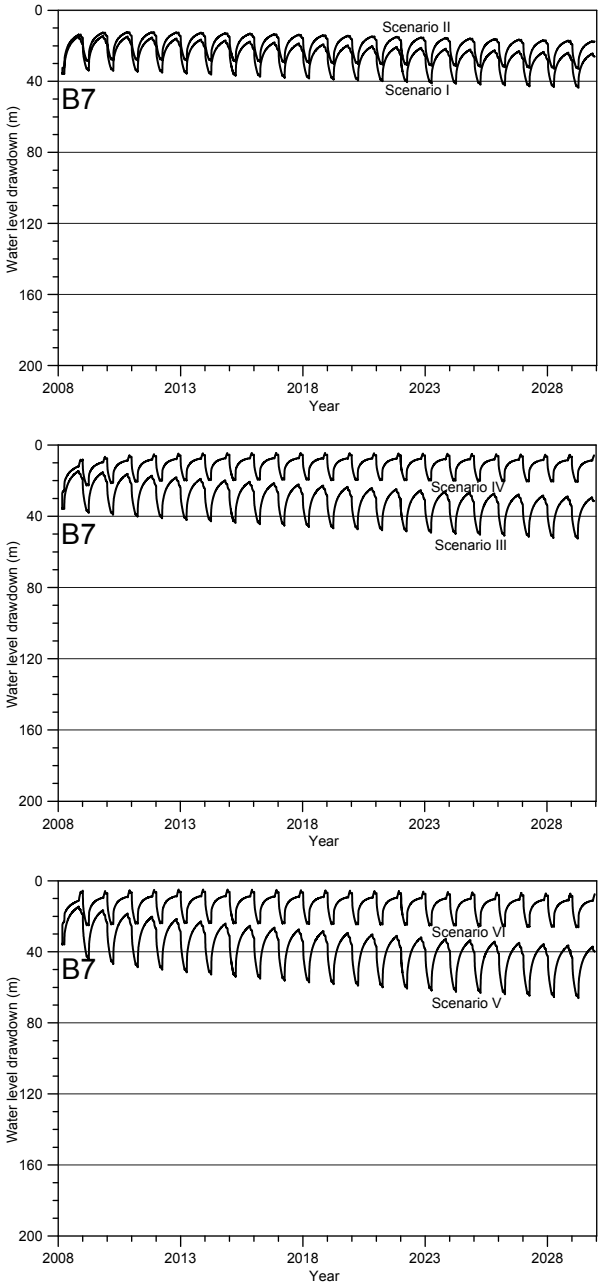

FIGURE 14: Predicted drawdown in well B7 for different scenarios

In contrast, the rate of drawdown was predicted to decrease when the reinjection ratio was 20% of the production and kept at a lower level when the reinjection ratio was increased to 50%. This does not only indicate a direct relationship between production and drawdown, but also shows the effect of the reinjection. Additionally, the water level recovery in well B7 was predicted to be higher than in other wells in the north, indicating a distant effect of reinjection (Figure 7).

Figure 15 shows that the drawdown in well O1 was predicted to increase from 60, 90 or 120 m at the end of 2030 when production is increased from 108, 129 and 162 l/s, without reinjection. When the reinjection plan was introduced, a predicted significant water level recovery was obtained in O1.

Continuous drawdown, caused by increasing production, and a remarkable water level recovery affected by the reinjection were predicted both in the northern and southern wells. Production rate, reinjection ratio and the distance between the reinjection well and production well were the three

factors that could influence the water level drawdown and recovery. The analysis above illustrates that a proper reinjection plan is undoubtedly a necessary and effective method to reduce pressure drawdown and even to maintain reservoir pressure.

4.1.2 Predicted pressure change in the entire field

Scenarios I, III and V in Figure 16 show that the water level in the geothermal field is predicted to be significantly affected by production, especially in the south and north where four small depression cones, due to concentrated pumping over the past 30 years, are predicted to become two larger depression cones when production is increased without reinjection. The drawdown in the nearby area of the reinjection wells is predicted to be higher than in the more distant area, indicating an obvious relationship between distance and drawdown. It is clear that the highest drawdown is predicted in the pumping centres due to the drastic production. The influencing range of pumping centres was predicted to grow with an increase in production; however, more mass flow from the surrounding area is predicted to be induced into the pumping centres, predicted to prevent a sharp drawdown occurring in the pumping centres but resulting in more drawdown in the surrounding area.

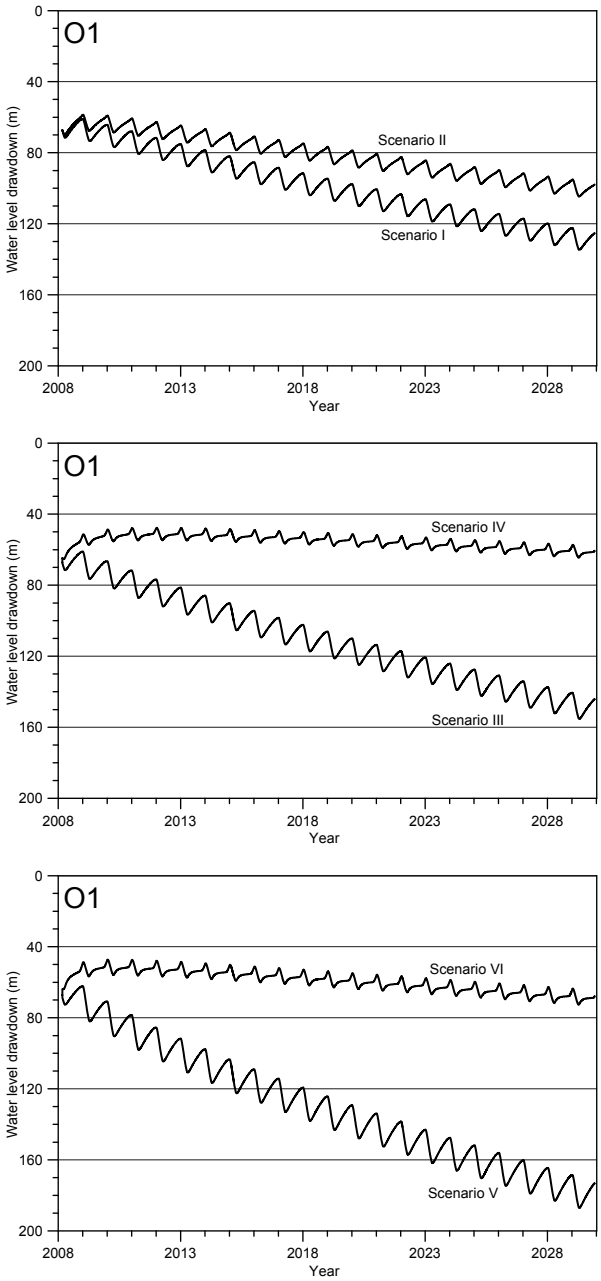

FIGURE 15: Predicted drawdown in well O1 for different scenarios

Scenarios II, IV and VI in Figure 16 illustrate a predicted water level recovery as well as drawdown, even in the areas far from the reinjection wells, which means that the reinjection is predicted to force the mass to flow centrifugally from the reinjection wells when there is mass flow from ambient areas to the pumping centres caused by production. The figure also shows that the influencing range caused by 50% reinjection is predicted to be larger than the range caused by 20% reinjection.

4.2 Predicted temperature change

Temperature change prediction was made by running flow and transport models in which 40°C geothermal water was re-injected into layer 6 in the north and south of the field over the next 20 years (Figure 17). Five non-production wells in the south and two non-production wells in the north were used for reinjection. Less than a 0.2°C temperature decrease was predicted to occur in production wells by the end of 2030 due to 108 l/s production with 20% reinjection (shown in Figure 18). Less cooling with 20% reinjection of the current production is predicted.

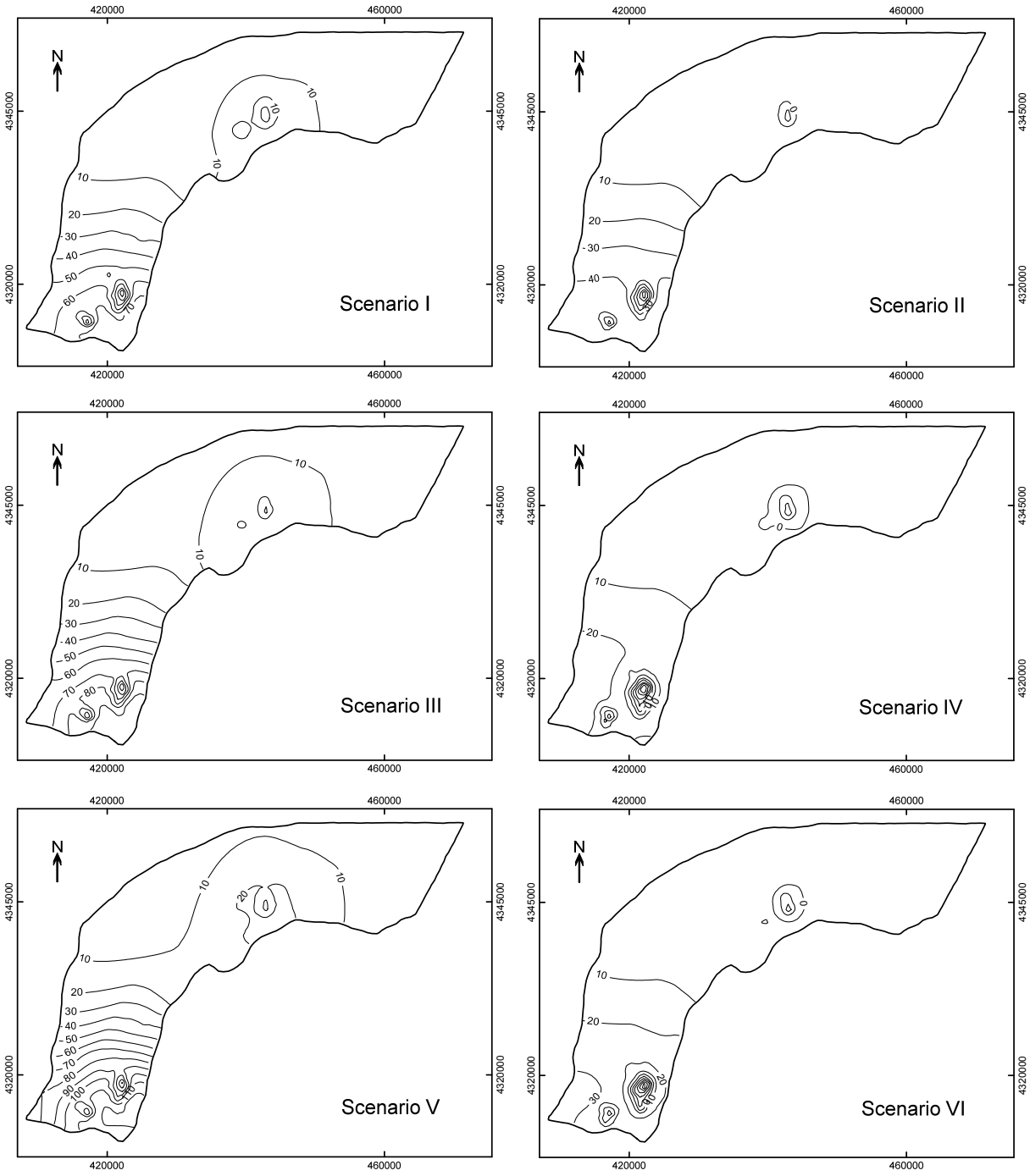

FIGURE 16: Predicted drawdown in the Niutuozhen field for different scenarios

Figure 19 shows that a temperature decrease ranging from 1.71 to 23.58°C is predicted in the reinjection wells from 108 l/s production rate with 20% reinjection. Cooling influence plumes are predicted to be gradually enlarged in the area surrounding the reinjection wells. The maximum temperature change is predicted to occur in the reinjection well sites. No change in temperature is predicted in other areas by reinjection within the geothermal field.

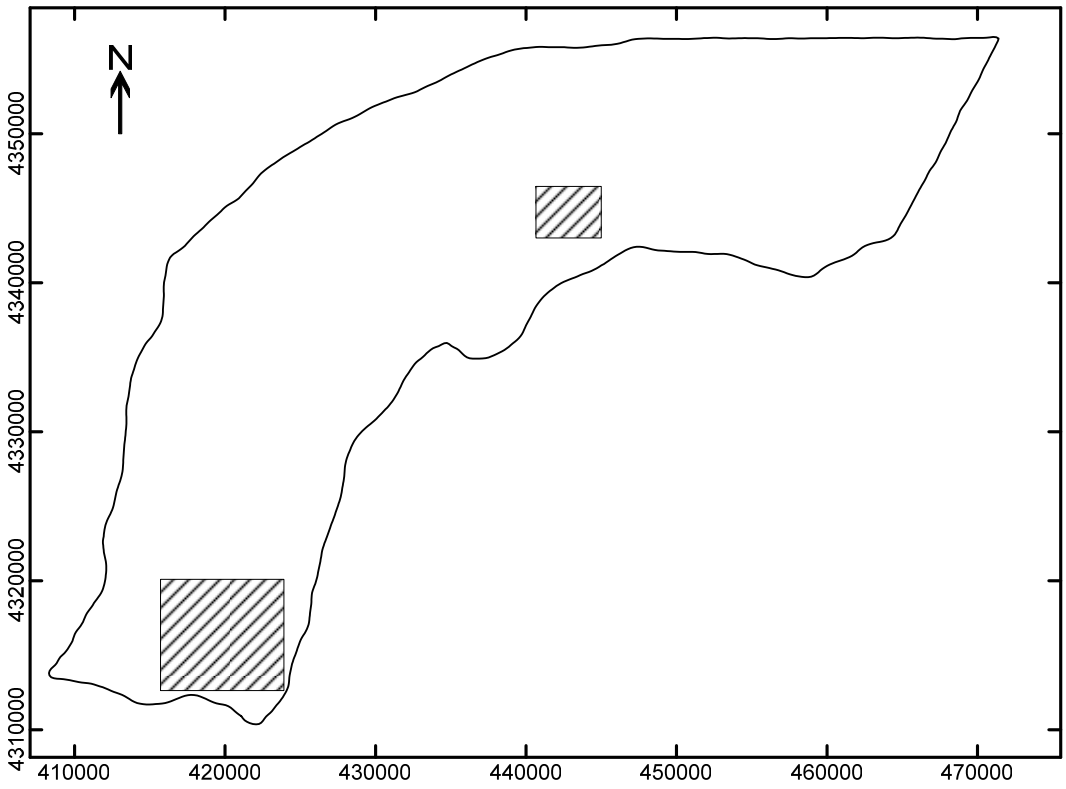

FIGURE 17: Reinjection well sites in the north and south

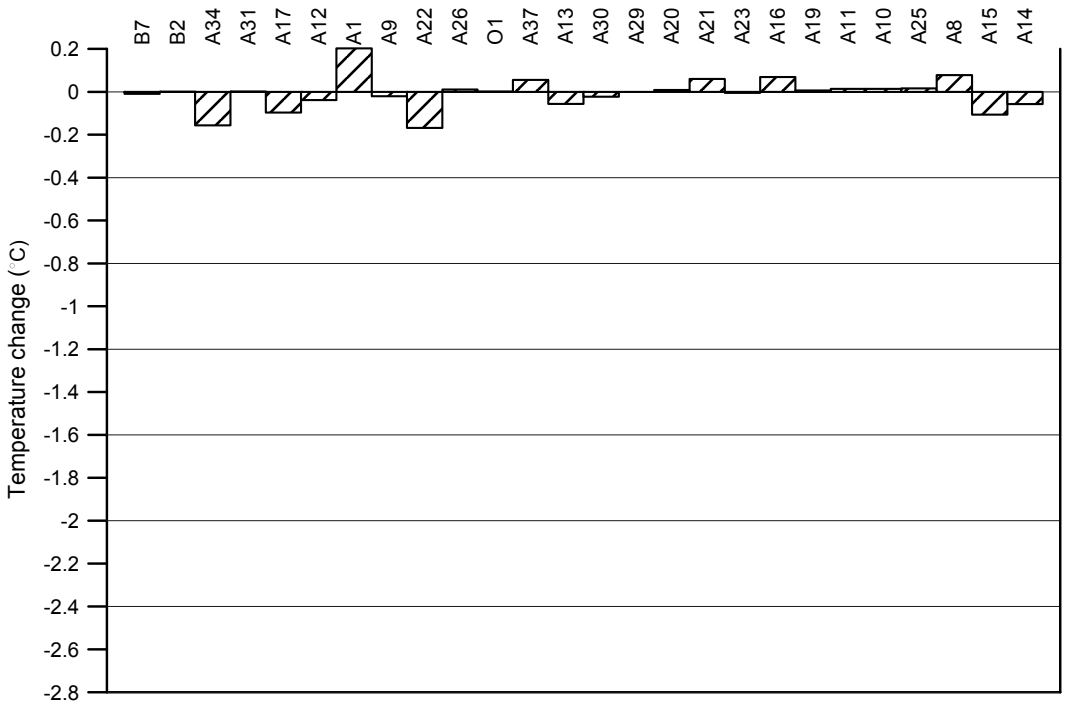

FIGURE 18: Predicted temperature change in production wells for scenario II

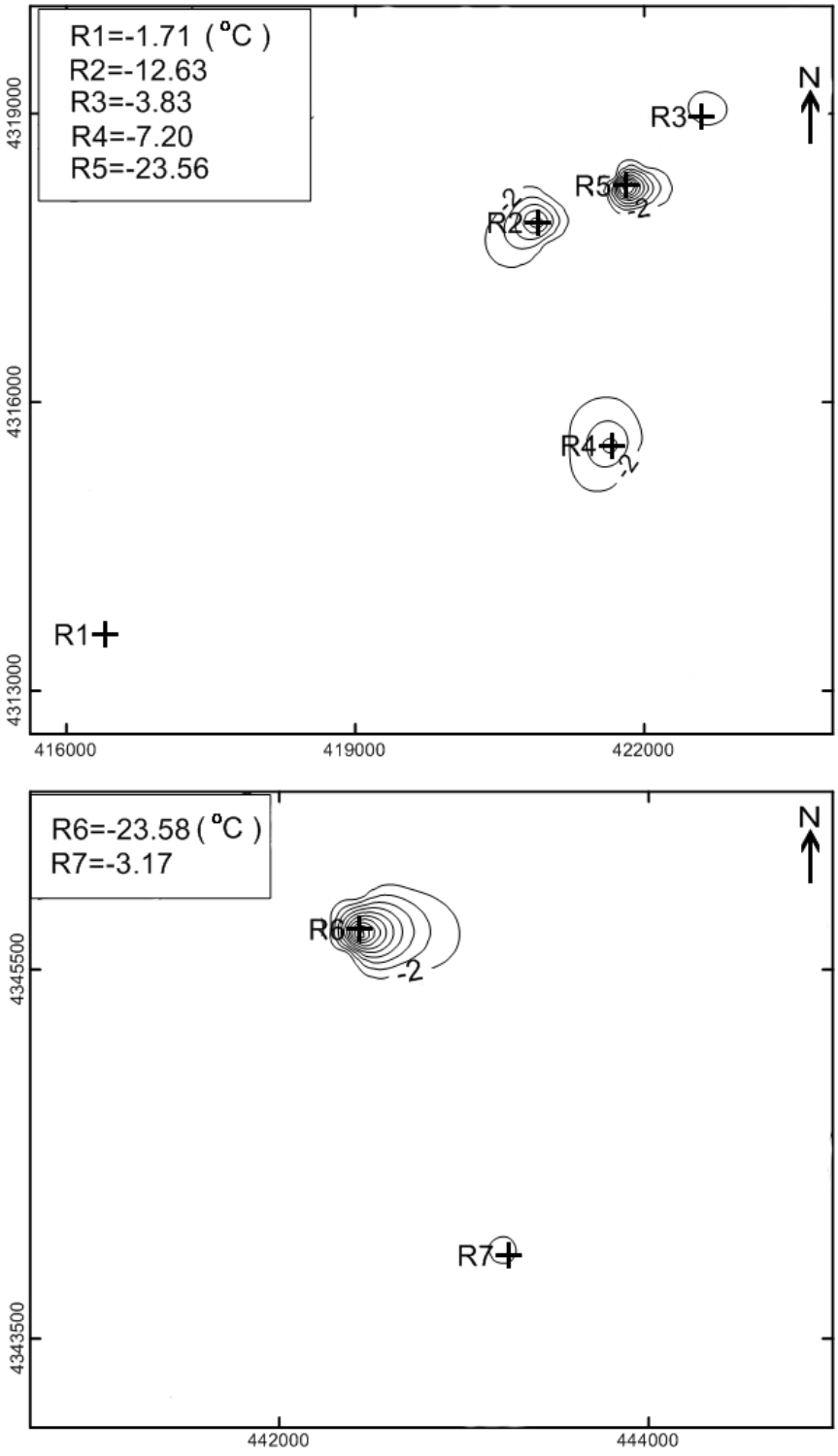

FIGURE 19: Predicted temperature change in the reinjection wells site for scenario II

When a production rate of 129 l/s with 50% reinjection is used, the cooling influence plumes are predicted to be slightly altered (Figure 20) when compared with the scenario based on 89 l/s production with 20% reinjection, as shown in Figure 19. Figure 21 shows that a noticeable temperature change is predicted in well A34, which is located 130 m from the R3 reinjection well while less than a 0.6°C temperature decrease is predicted in wells A22, A12 and A17, which are close to reinjection wells R5 and R3.

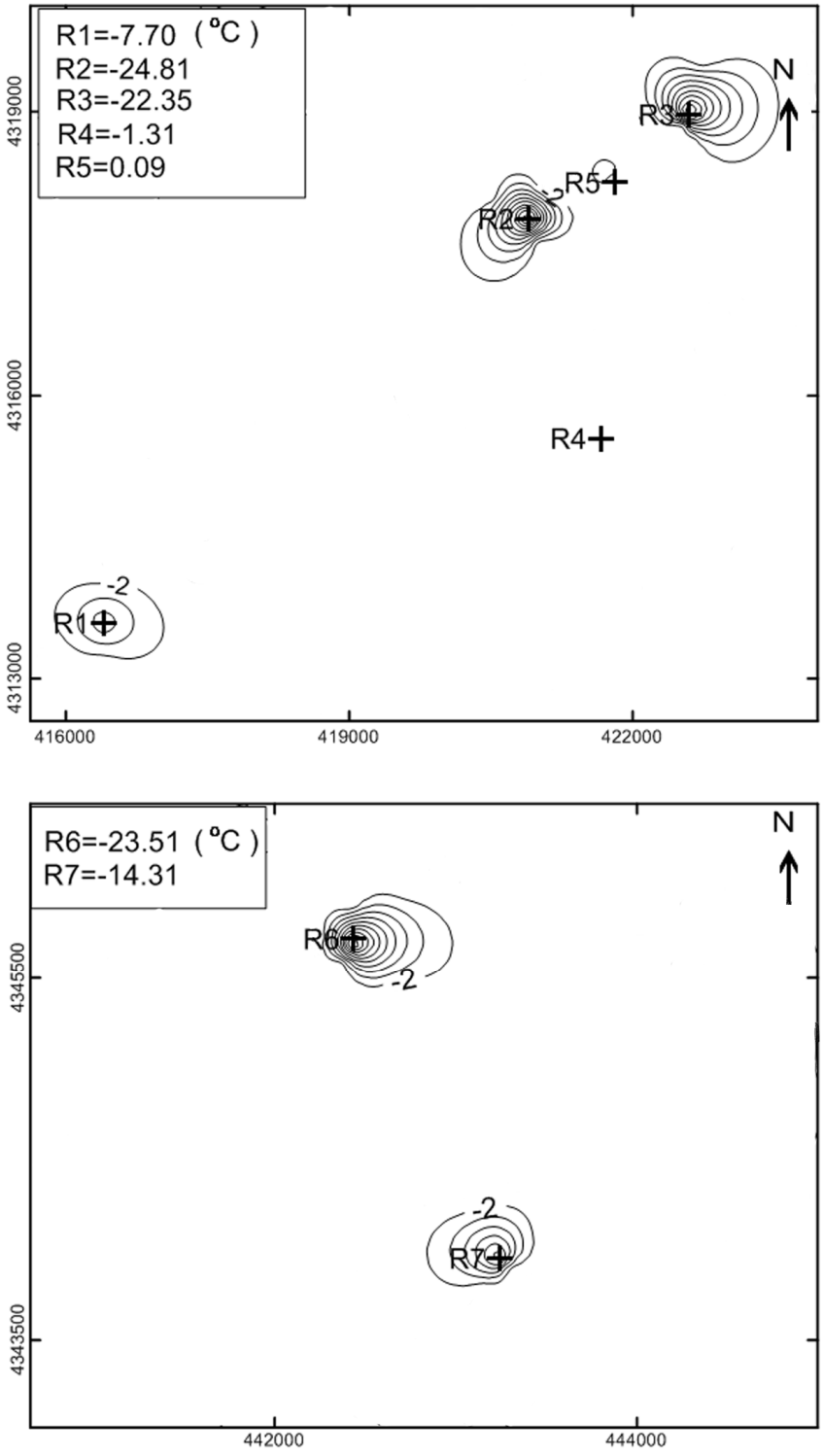

FIGURE 20: Predicted temperature change in the reinjection wells site for scenario IV

Figure 22 shows that temperature change increases in wells A34, A22, A12 and A17, which are close to reinjection wells R5 and R3 with a 160 l/s production and 50% reinjection. There is no obvious change in the cooling influence plumes, as shown in Figure 23 when compared with the scenario based on 129 l/s production with 50% reinjection, as shown in Figure 21.

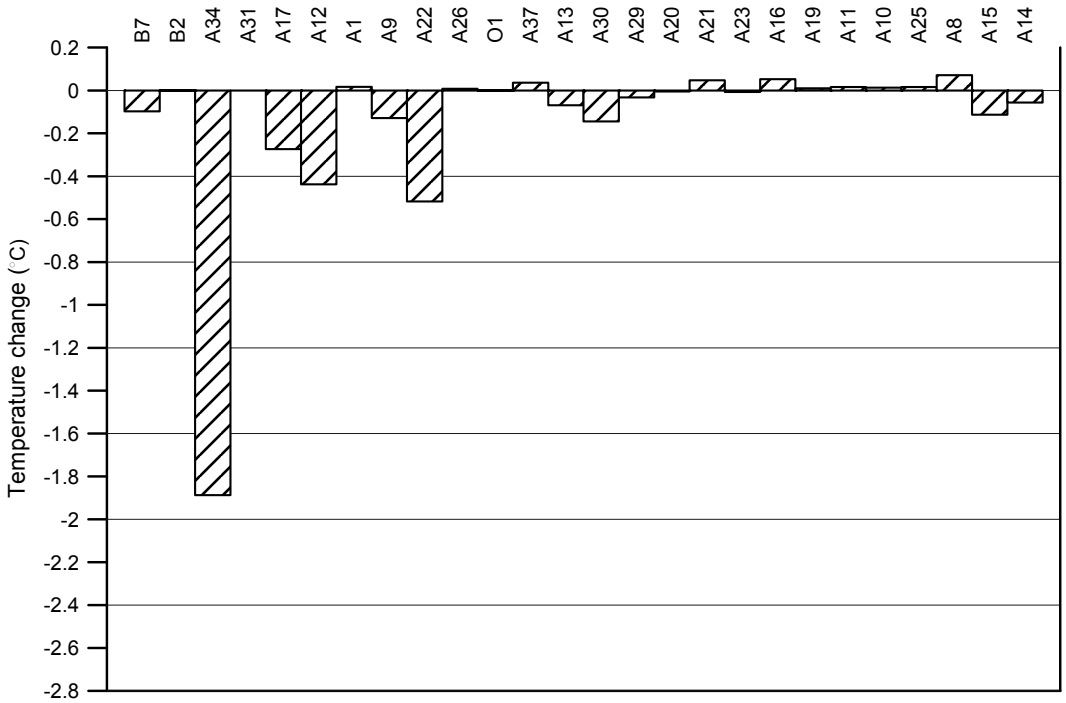

FIGURE 21: Predicted temperature change in production wells for scenario IV

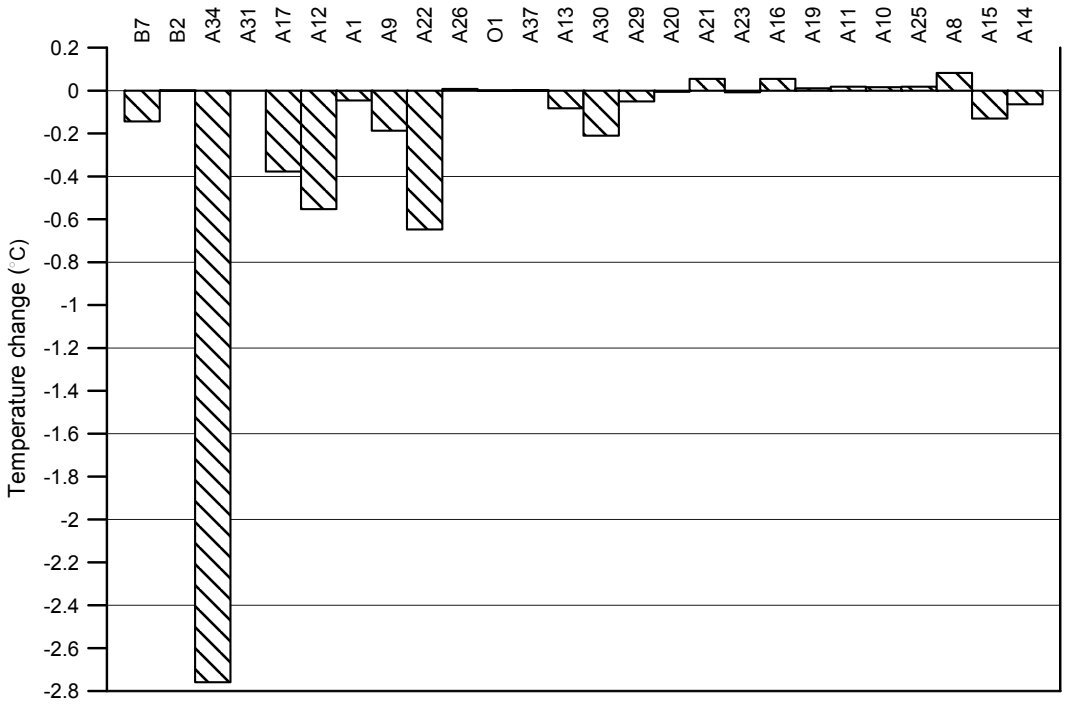

FIGURE 22: Predicted temperature change in production wells for scenario VI

The highest temperature changes were predicted at the sites of reinjection wells due to continuous reinjection with 40°C water for the next 20 years. The influencing range of cooling plumes was predicted to grow when reinjection is increased from 20 to 50%. Less than a 2.8°C decrease was predicted in all the production wells, but the most obvious change among the production wells was predicted in A34 (from -0.18 to -2.75°C) which is located near reinjection well R3. Based on the

above analysis, the distance between the reinjection wells, reinjection rate and temperature of reinjection water are the major concerns for reinjection cooling danger.

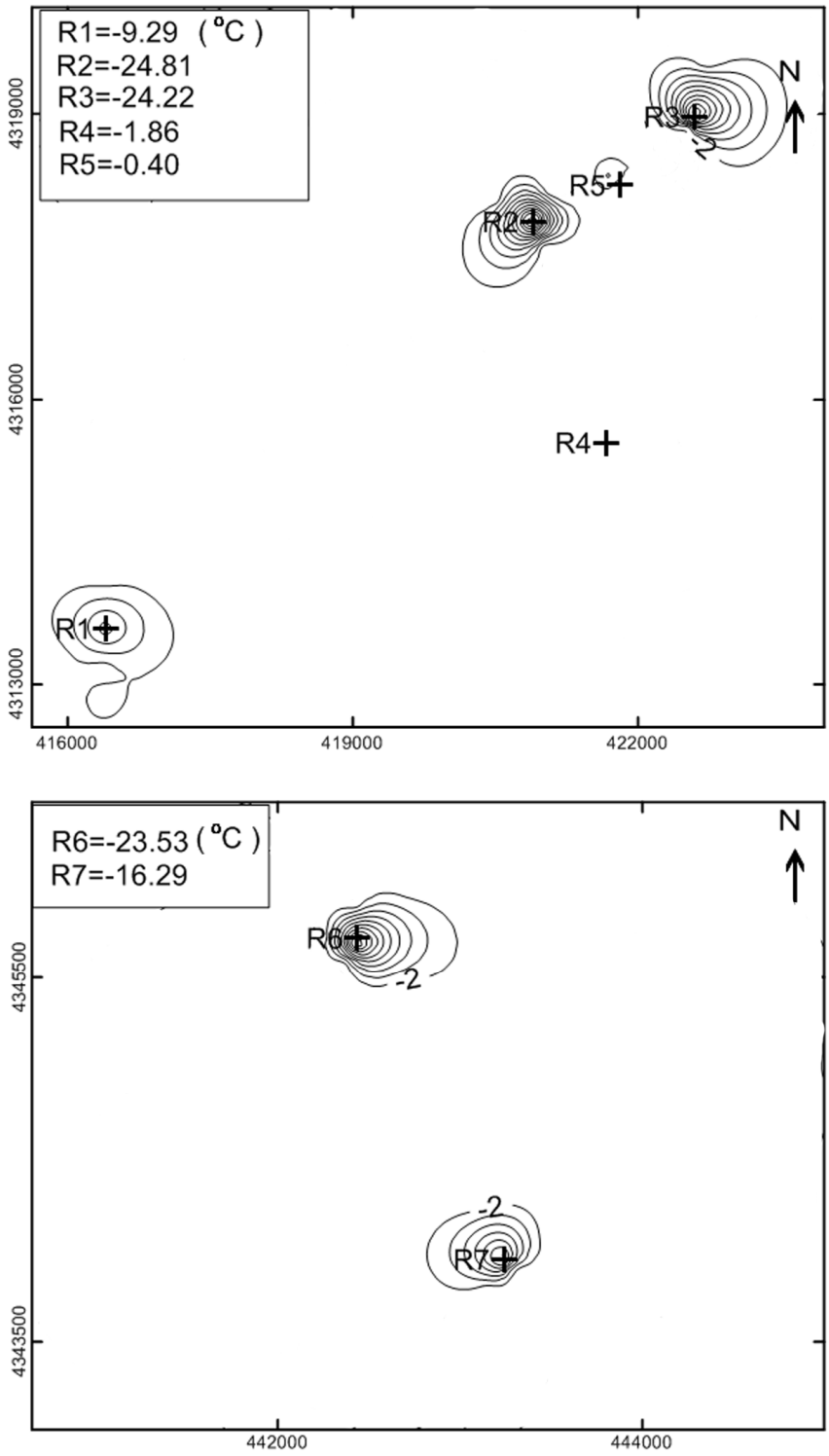

FIGURE 23: Predicted temperature change in the reinjection wells site for scenario VI

5. CONCLUSIONS AND RECOMMENDATIONS

The Niutuozhen geothermal field system located in North China is composed of two reservoirs, the Jixian system dolomite reservoir and the Neogene sandstone reservoir. A three-dimensional model with 5437 elements and seven layers based on geological and geothermal data of the Niutuozhen geothermal system was built using the AQUA3D package which was designed for solving flow and transport problems. An area of 1050 km^2 confined by four faults is included in the model. The focus was on layer 6, from which most of the current production wells are pumping. Production history of forty five wells and pressure monitoring data from six wells were used for calibrations. Permeability was estimated from 2.5 to 25×10^{-16} m^2 in layer 6 after a satisfying agreement was obtained between the available measured and computed water level data.

Reservoir performance, both in pressure and temperature corresponding to six scenarios with different production rates and reinjection ratios, was predicted. When using 162 l/s as the production rate without any reinjection, the maximal drawdown in the north and south ranges from 30 to 120 m, respectively, after 20 years of production. The rate of drawdown is predicted to be kept at a lower level if the production rate is 129 l/s with 50% reinjection. Cones of depression in the southern town Xiongxian and northern town Gu'an are predicted to gradually enlarge due to an increased production rate without reinjection, but are effectively limited and even diminished when the proposed reinjection ratio is 50%.

A maximum temperature decrease of 2.75°C is predicted to occur in production well A34, located near reinjection well R3, when the production rate is 162 l/s with 50% reinjection in the southern town, Xiongxian. The maximal temperature decrease in other production wells is predicted to be less than 0.8°C when reinjection is carried out. The maximum temperature decrease of 24.81°C is predicted to occur in the southern reinjection well R2 when using a 129 l/s production rate with 50% reinjection, and 162 l/s with 50% reinjection. The cooling plumes surrounding the reinjection wells are predicted to gradually enlarge with an increase in reinjection ratios. Predictions of the temperature response, according to the different scenarios with reinjection, indicate that the reinjection ratio, the temperature of the reinjected water and the distance between the reinjection and production wells are so vital that large scale reservoir cooling may be induced if these three factors are not considered carefully before reinjection.

In the future, a reinjection plan is necessary in order to achieve sustainable development of the geothermal resources in the Niutuozhen field. More water level monitoring points are needed in the south and detailed data should be collected at lease monthly in the north.

ACKNOWLEDGEMENTS

I would like to thank the government of Iceland and the United Nations University Geothermal Training Programme for supporting me to accomplish this training. Thanks to all the staff of the UNU-GTP, especially Dr. Ingvar B. Fridleifsson, Director, and Mr. Lúdvík S. Georgsson, Deputy Director. Sincere thanks to my advisor, Mr. Andri Arnaldsson, who has given me valuable comments on my project and the final report, and Mr. Eric M. Myer, Mr. Snorri Páll Kjaran and Dr. Gudni Axelsson, who helped me a lot with my project. I would like to give special thanks to Dr. Liu Jiurong and Prof. Pang Zhonghe, who shared their perfect academic knowledge with me. Finally, I am grateful to the other UNU Fellows, MSc Fellows and PhD Fellows for their helpful opinion on my project.

REFERENCES

Chen M., 1988: *The geothermal field in the North China plain, China* (in Chinese). Science Publisher, Ltd., Beijing, 218 pp.

Chen M., Deng X., Wang J., and Wang J., 1985: On the formation and accumulation of thermal water in Norht China plain (in Chinese with English abstract). *Earth Science, 10-1*, 83-90.

Chen M., Huang G., Zhang W., and Zhang W., 1982: The temperature distribution pattern and the utilization of geothermal water at Niutuozhen basement protrusion of central Hebei province (in Chinese with English abstract). *Scientia Geologica Sinica, 3*, 239-252.

Geothermal Group, 1983: A preliminary investigation on the characteristics of a geothermal field and the conditions for its formation in the northern part of the North China Plain (in Chinese with English abstract). *Bulletin of the 562 Comprehensive Geological Brigade, Chinese Academy of Geological Sciences, 4*, 109-126.

Hu S., 1994: Distributed parameter model for the Zhangzhou geothermal field, China. Report 3 in: *Geothermal Training in Iceland 1994*. UNU-GTP, Iceland, 53-68.

Liu J., Wang S., and Lin P., 2005: *The geothermal resource assessment report in Xiongxian geothermal field, Hebei Province, China.* Beijing Institute of Geological Engineering, Beijing, China, report (in Chinese), 65 pp.

Ma J., Cai H., Zhang D.,Yan G., and Chang F., 1990: *Survey report of the Niutuozhen geothermal field*. The 3rd Hydrogeological and Engineering Geological Brigade of Hebei Province, Hebei province, China, report (in Chinese), 216 pp.

Qi J., Yang Q., Lu K., Zhou J., and Wang Z., 2004: Geologic map of sub-outcrop and its implied information of tectogenesis in Bohai Bay basin province (in Chinese with English abstract). *Earth Science Frontiers, 11*, 300-307.

Vatnaskil, 1998: *AQUA3D user's manual.* Vatnaskil Consulting Engineers, Reykjavík, 86 pp.

Wu Y., and Pruess K., 1998: A 3-D hydrodynamic dispersion model for modeling tracer transport in geothermal reservoirs. *Proceedings of the 23rd Workshop on Geothermal Reservoir Engineering. Stanford, Ca.,* 139-146.

Zhou R., 1987: The activity of deep underground water in the northern part of the North China Plain and its effect on the geothermal field (in Chinese with English abstract). *Bulletin of the 562 Comprehensive Geological Brigade, Chinese Academy of Geological Sciences, 6*, 17-36.

Zhou R., Liu Q., Zhang J., and Yang L., 1989: The geological features and exploitive prospects of the geothermal field of salient type bed rock of Niutuozhen in the fault basin of North China (in Chinese with English abstract). *Bulletin of the 562 Comprehensive Geological Brigade, Chinese Academy of Geological Sciences, 7-8*, 21-36.